Pointer Image Theory Usage for Common Mode Current Prediction at Power Lines

M.Sc. Muhammad S. Alamsyah, Leibniz Universität Hannover, Germany
M.Sc. Francinei Vieira, Leibniz Universität Hannover, Germany
Prof. Dr.-Ing. Sebastian Koj, Jade University of Applied Science, Germany
Prof. Dr.-Ing. Heyno Garbe, Leibniz Universität Hannover, Germany

Abstract

This paper aims to explain the pointer image theory as a solution used to predict the common mode (CM) current at power lines, which is strongly related to radiated electromagnetic emissions. Techniques to measure the CM current at power lines in huge installations such as wind turbines (WT) are needed and novel methods are emerging. The WT tower may become an unintentional antenna due to the CM current flowing at its body through stray capacitances. The easiest way to measure the total CM current flow on a three-phase system is by measuring it using a device such as a current clamp or a Rogowski coil. This clamp must cover the whole 3-phase-cable bundle, however, the problem is that such a huge clamp or coil does not exist on the market, besides customized parts. The proposed method in this paper is to implement the pointer image theory to predict the CM current from a WT power plant. Laboratory measurements and SPICE simulations are used to show that the proposed method works well for CM current prediction.

Keywords: Common Mode current measurement, pointer image theory, current clamp, power lines

1 Introduction

In the era of an increasing need to use green energy, the installation of renewable energies is happening rapidly to answer the global warming issue that has been happening until today. There are many power plant options used such as photovoltaic, wind energy, hydro, biomass, etc. Some of those power plants have caused several electromagnetic compatibility (EMC) issues [1]. This paper focuses on highlighting the wind turbine (WT) case. It has been considered as an unintentional antenna due to the common mode (CM) current flowing at its body [2]. Measurement of CM current and its radiated magnetic field emission showed a great agreement between each other [3]. The position of the current probe along the cables of a WT affects the measurement results, due to the occurrence of standing waves [4]. The radiated emission attenuation from the steel tower is discussed in [5]. The discussion about both conducted and radiated emission at WT from different causes is covered in detail in [6]. The radiated emission from the WT should not disturb the radio broadcast services or the navigation systems, which are regulated by the EU Directive [7].

Stray capacitance is formed between the transmission line conductors and the WT body, allowing a link between them for the flow of CM current. At the kHz switching frequency level of the power converter, the impedance of the stray capacitance is decreasing, so that the continuous CM current is flowing and causing the huge – e.g. 100 meters – WT body acting as a monopole antenna. The easiest way to measure the CM current flowing, in this case, is by putting a big current clamp or a Rogowski coil covering the whole conductor bundles, but such a humongous clamp does not exist on the market or might be a custom-made one. This paper proposes a

This project has received funding from the European Union's Horizon 2020 research and innovation program under the Marie Skłodowska-Curie grant agreement No 812753.

measurement method that use smaller current clamps to cover each phase conductor bundle and, by applying the pointer image method with some combinations, the CM current could be obtained by only measuring the magnitude of the current, which was previously discussed in [8]. This approach is performed with two different simple circuits representing the model of a WT's body. Simulations using SPICE software and a laboratory measurement are implemented and the results are compared.

2 Pointer Image Theory

The pointer image theory is a vector construction technique of multi-phase currents with their phase angles. The pointer image itself is different between a balanced and an unbalanced system. The balanced system's pointer image will show only three pointers as shown in Figure 1a. Unlike Figure 1a, the unbalanced system's pointer image will have an extra pointer (between the end pointer of phase 3 pointer and the starting point of phase 1 pointer) which depicts the unbalance current as shown in Figure 1b. The length of it is considered as the CM current magnitude. The magnitude and its phase angle are the sums of all of the phases' current magnitudes and their phase angles as stated in Equation 1. The term unbalanced current is usually used in power system engineering, but in the EMC perspective, we will consider it as a CM current.

$$\underline{I}_1 + \underline{I}_2 + \underline{I}_3 = \underline{I}_{CM} \tag{1}$$

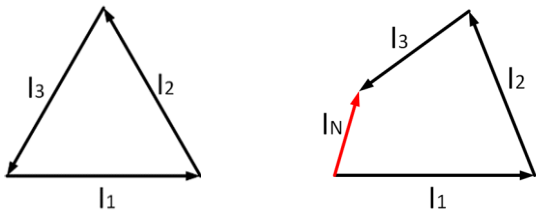

(a) (b)

Figure 1: Pointer Image for: (a). A Balanced 3-Phase system and (b). Unbalanced 3-Phase System

For a three-phase, four-wire system, the unbalanced or the CM current will flow at the fourth wire, so in order to know the CM current value, measuring the current flowing at the fourth wire is sufficient. In the case of WT, the transmission line is connected in delta, so there is no fourth wire. The CM current will flow at the WT body as mentioned before through the stray capacitances. The proposed method in this paper is done by performing the following magnitude-only measurements, as shown in Figure 2:

A. Each phase current (P1, P2, and P3)
B. Bundle phase current (P1+P2 and P2+P3)

(a) (b)

Figure 2: Illustration of the current clamp placement – in red – for the measurements, (a) 1-phase measurement, and (b) phase bundle measurement

By obtaining those 5 measurements results, the vectors based on the pointer image theory could be constructed. The advantages of using this method are, first, the image reconstruction only needs the current magnitude without the phase angle, and second, the measurements could be done at the power cable using a smaller current clamp or Rogowski coil that can cover only a 2-phase bundle. This, of course, provides advantages not only on the measurement procedure – with simple and practical steps – but also economic due to the current clamp sizes available commercially. This method will be used to predict the CM current on 2 different circuits to show its high degree of confidence.

3 Circuit Modeling

To show how the prediction works, two simple representation circuits are used. The first circuit is a three-phase, four-wire system and the second circuit is a three-phase, three-wire system. The conductor inside the WT will be constructed as shown in Figure 3. The conductors are arranged in a perfect triangle and located on top of a plain surface (ground plane). The plain surface is a representation of the WT body. The huge scale difference between the distance of phase-to-phase conductors to the phase-to-ground distance is used as an assumption for the flat plain surface rather than circular surface like the real WT. The predictions were carried out by a laboratory measurement for circuit 1 and SPICE simulation for circuit 2 which adapts the conductor arrangement on Figure 3.

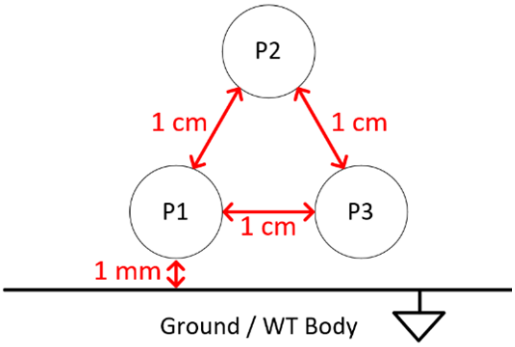

Figure 3: Conductor arrangement

3.1 Circuit 1

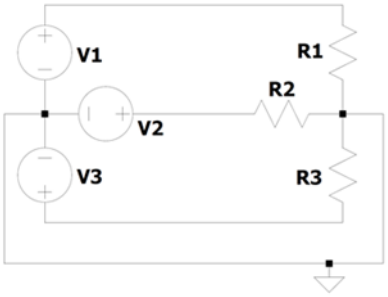

Figure 4: Circuit 1

The first circuit is a three-phase, four-wire circuit, shown in Figure 4. The source and load are both connected in star connection. It uses a three-phase sinusoidal voltage source with 67 V magnitude, 50 Hz frequency, and 120° phase difference between each phase. The transmission line which connects the source and the load is modeled as a lossless transmission line to show a simplified circuit and focus on the flow of the CM current due to the unbalanced load. It will then be applied to the pointer image theory for the prediction of the CM current.

The loads are varied into 5 different combinations to cause the neutral current to flow at the 4th wire. The loads are summarized in Table 1.

	Resistance of Each Variation Type				
Component	Type 1	Type 2	Type 3	Type 4	Type 5
P1 Load	46 Ω	69 Ω	16 Ω	92 Ω	62 Ω
P2 Load	32 Ω	76 Ω	46 Ω	62 Ω	46 Ω
P3 Load	76 Ω	92 Ω	76 Ω	32 Ω	16 Ω

Table 1: Load Variations

3.2 Circuit 2

The second circuit is a three-phase, three-wire circuit. A slight modification is made from the first circuit, the source is connected in star connection and the load is connected in delta connection. The source is a balanced three-phase rectangular source with a fundamental frequency of 10 kHz. It is connected to a ground (WT body) represented as a 4th wire, as can be seen in Figure 5. The load is balanced. The transmission line is connected to the WT body through the stray capacitance. The stray capacitance value will be obtained through Equation (2) [9]. Based on Figure 3, we knew that the position of the phase 2 conductor to the ground is different from the other two phases. This will result in a different stray capacitance value among them, as shown in Table 2, and this unbalanced capacitance will be observed in its effect on the flowing CM current. The distances between the phase conductors to the ground will further be varied to observe the behavior of CM current under different stray capacitance values.

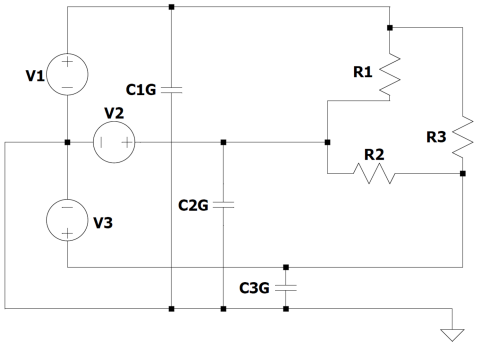

Figure 5: Circuit 2

$$C = \frac{2\pi\varepsilon_0 l}{\ln\left(\frac{2a}{r}\right)} \quad (2)$$

ε_0 Vacuum Permittivity
l Wire Length (m)
a Distance between cable core to the ground (m)
r Wire radius (m)

Distance	C1G & C3G	C2G
1 mm	41.457 pF	17.692 pF
5 mm	23.084 pF	16.273 pF
1 cm	18.485 pF	15.113 pF
5 cm	12.257 pF	11.767 pF
10 cm	10.653 pF	10.453 pF

Table 2: Capacitances for Different Distances to the Ground

4 Results and Analysis

4.1 Circuit 1

	Value in A				
Current	Type 1	Type 2	Type 3	Type 4	Type 5
P1	1.500	1.140	3.820	0.750	1.090
P2	2.000	0.910	1.420	1.090	1.500
P3	0.930	0.760	0.930	2.000	3.970
P12	1.790	1.050	3.350	0.988	1.380
P23	1.760	0.850	1.350	1.740	3.440
CM	0.920	0.330	2.700	1.120	2.660

Table 3: Current Measurement Using Current Clamp

The unbalanced loads cause a flow of CM current, which will be used to check the prediction accuracy of the pointer image theory. The current measured by the clamp for each phase and 2-phase bundles are summarized in Table 3. Those 5 current measurements are used to recreate the pointer image, which is then used to predict the CM current. The CM current obtained from the measurement and pointer image prediction are summarized in Table 4. The differences given by the pointer image method are all below 1% which is quite accurate. It could then be assumed that the method is precise enough to predict the CM current flowing at the 3-phase system. Based on this high accuracy, this method is used on circuit 2, which simulates the CM current flowing from the WT transmission lines to its body.

	Value in mA				
CM Current	Type 1	Type 2	Type 3	Type 4	Type 5
Measurement	0.920	0.330	2.700	1.120	2.660
Pointer Image	0.927	0.332	2.708	1.112	2.657
Difference	**0.76%**	**0.61%**	**0.30%**	**0.71%**	**0.11%**

Table 4: Pointer Image Prediction for the Neutral Currents

4.2 Circuit 2

Using the same sequence at circuit 1, the current measurements for each phase and the CM current for circuit 2 modeled in a SPICE simulation are given in Table 5. The CM current from circuit 2 is observed not only at 10 kHz frequency but also for other frequencies. Those are 110 kHz, 430 kHz, 670 kHz, 850 kHz, and 1.09 MHz. The purpose of observing at those higher frequencies is to prove that the pointer image CM current prediction works on every frequency so that the method could be used for a broad purpose. The results below used stray capacitance with a 1 mm distance between phases 1 and 3 regarding the ground. The other 4 variations are covered in the next subsection.

	Current in mA					
Frequency	10 kHz	110 kHz	430 kHz	670 kHz	850 kHz	1,09 MHz
P1	1,309	137.517	66.981	63.328	62.358	61.728
P2	1,291	140.682	19.712	16.120	16.280	16.930
P3	1,336	98.217	60.184	50.807	47.546	45.121
P12	1,339	95.616	63.331	53.925	50.642	48.190
P23	1,308	136.624	63.943	60.208	59.229	58.604
CM Current	3.163	3.167	3.149	3.140	3.134	3.124

Table 5: Currents Measurement from LTSPICE Simulation

	CM Current in mA					
Frequency	10 kHz	110 kHz	430 kHz	670 kHz	850 kHz	1,09 MHz
Simulation	3.163	3.167	3.149	3.140	3.134	3.124
Pointer Image	3.074	3.167	3.149	3.140	3.133	3.124
Difference	**2.81%**	**0.00%**	**0.00%**	**0.00%**	**0.03%**	**0.00%**

Table 6: CM Current Prediction using Pointer Image for Circuit 2

In Table 6, the pointer image predictions for the CM current are given. Those currents caused by the unbalanced stray capacitance due to the different positions of the WT transmission lines referred to the ground, are precisely predicted by the pointer image theory. At 10 kHz, the difference is 2.81% which is caused by the phase currents and CM current scale difference. The phase currents are in the order of *amperes* (A) while the CM current is in the order of *milliamperes* (mA), as seen in Table 5. The 10^3-scale difference is the weak point of this method, but for the other frequency points, which are below the 10^3-scale difference, provided accurate predictions.

4.3 CM Current Under Different Stray Capacitances

In this subsection, the CM current behavior under different stray capacitances is observed. The variation of the stray capacitances is summarized in Table 2. The distance between each phase of the transmission lines to the ground is increased in such a manner to observe how it affects the CM current at the WT. It can be seen in Figure 6. that when the stray capacitance is decreased due to the increased distance, the CM current at the WT will reduce. It is caused by the increasing impedance of the stray capacitance.

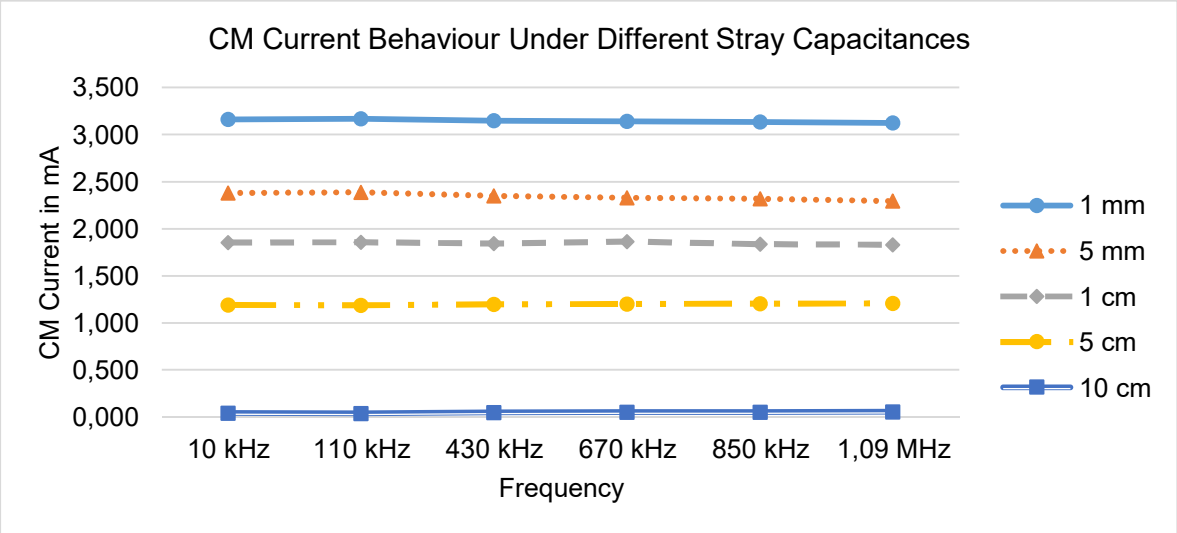

Figure 6: CM Current Behaviour Under Different Stray Capacitances

5 Conclusion

This work demonstrated a practical implementation of the pointer image theory to predict the CM current from a WT power plant, supported with simulations and measurements with excellent agreement between them and for a considerable frequency range. The observed results indicate that the CM current flowing at the WT body is greatly impacted by the stray capacitance and, therefore, this must be considered when designing such WT or equivalent system, so that the potential radiated emissions caused by the CM current could be decreased or controlled since the design phase.

References

[1] FUNABASHI, Toshihisa, YAMAMOTO, Kazuo and SEKIOKA, Shozo, 2018. Lightning protection and EMC issues of renewable energy sources. In: *IEEE International Symposium on Electromagnetic Compatibility and IEEE Asia-Pacific Symposium on Electromagnetic Compatibility (EMC/APEMC)*. IEEE. 2018. p. 805–810, doi: 10.1109/ISEMC.2018.8393892.

[2] FISAHN, Sven, PHAM, Hoang Duc, SANDMANN, Sergei, GARBE, Heyno and KOJ, Sebastian, 2019. Far Field Region of Radiated Emissions from Wind Energy Conversion Systems. In: *2019 International Symposium on Electromagnetic Compatibility - EMC EUROPE*. IEEE. September 2019. p. 450–455. doi: 10.1109/EMCEurope.2019.8872081.
[3] KOJ, Sebastian, FISAHN, Sven and GARBE, Heyno, 2016. Determination of radiated emissions from wind energy conversion systems. In: *2016 International Symposium on Electromagnetic Compatibility - EMC EUROPE*. IEEE. September 2016. p. 188–192. doi: 10.1109/EMCEurope.2016.7739262.
[4] KOJ, Sebastian, RESCHKA, Cornelia, FISAHN, Sven and GARBE, Heyno, 2017. Radiated electromagnetic emissions from wind energy conversion systems. In: *2017 IEEE International Symposium on Electromagnetic Compatibility & Signal/Power Integrity (EMCSI)*. IEEE. August 2017. p. 243–248. doi: 10.1109/ISEMC.2017.8077874.
[5] KOJ, Sebastian, FISAHN, Sven and GARBE, Heyno, 2018. Simplified Procedure to Predict the EM Emissions of Wind Energy Conversion Systems. In: *2018 IEEE Symposium on Electromagnetic Compatibility, Signal Integrity and Power Integrity (EMC, SI & PI)*. IEEE. July 2018. p. 423–426. doi: 10.1109/EMCSI.2018.8495243.
[6] CIGRE WG C4.30, 2017. *EMC in Wind Energy Systems*. Tech. Rep. n.707. CIGRÉ.
[7] *Directive 2014/30/EU of THE EUROPEAN PARLIAMENT AND OF THE COUNCIL of 26 February 2014 on the harmonization of the laws of the Member States relating to electromagnetic compatibility*. [online]. Available from: http://data.europa.eu/eli/dir/2014/30/oj
[8] ALAMSYAH, Muhammad S., VIEIRA, Francinei L., GARBE, Heyno and KOJ, Sebastian, 2021. The Effect of Stray Capacitance to the Common Mode Current on Three-Phase System. In: *2021 IEEE International Joint EMC/SI/PI and EMC Europe Symposium*. IEEE. 26 July 2021. p. 430–433. doi: 10.1109/EMC/SI/PI/EMCEurope52599.2021.9559135
[9] HERING, Ekbert, MARTIN, Rolf, STOHRER, Martin and KÄSS, Hanno, 2016. Elektrizität und Magnetismus. In: *Physik für Ingenieure*. Berlin, Heidelberg: Springer Berlin Heidelberg. p. 237–375. ISBN 978-3-662-22292-8.